The Concept of Mean Free Path in the Kinetic Monte Carlo Description of Bulk Fluid Behaviour, Vapour-Liquid Equilibria and Surface Adsorption of Argon

by

Chunyan Fan, D. D. Do* and D. Nicholson
School of Chemical Engineering
University of Queensland
St. Lucia, Qld 4072
Australia

Abstract

Recently, kinetic Monte Carlo simulation (*kMC*) has been successfully applied to describe bulk fluid behaviour, vapour-liquid equilibrium and adsorption on a graphite surface [1]. Its advantage over Metropolis-Monte Carlo lies in the excellent sampling of the energy space for the direct determination of the chemical potential. In this paper, we address the mechanics of the displacement of a particle, which is the only step in *kMC*. By invoking the mean free path concept and the average travel distance, we establish the connection between the particle sampling of the volume space and the distance of travel of the particle related to the mean free path through the Beer-Lambert law. We apply this procedure to vapour-liquid equilibrium in bulk fluid argon, and to adsorption of argon on a graphite surface, and demonstrate that the results are entirely consistent with previous simulations.

Keywords: Kinetic Monte Carlo; mean free path; bulk fluid behaviour; vapour-liquid equilibrium; surface adsorption

Author to whom all correspondence should be addressed; Email: d.d.do@uq.edu.au

1. Introduction

Monte Carlo (*MC*) simulations with the Metropolis algorithm (importance sampling) [2, 3] have been widely used in studying equilibrium properties of bulk fluids and adsorption systems [4-10]. A new scheme, which has its basis in a kinetic Monte Carlo (*kMC*) method, has recently been introduced to study bulk fluid behaviour and vapour-liquid equilibrium, and it has shown great promise as an alternative to Metropolis *MC* [1]. One distinct advantage of *kMC* is that no moves are rejected in any *kMC* step, and therefore the energy space is sampled with real particles; a consequence being that the chemical potential is calculated very efficiently. The only basic move in the *kMC* method is the selection of a particle based on its mobility and its movement to a random position (uniform sampling) within the simulation box [1] which allows the system to evolve rapidly to an equilibrium state. To provide a basis for this *kMC* step we introduce in this paper a concept of mean free path (*MFP*), which recognizes the density dependence of the mean distance between molecular collisions. We explore a number of schemes that determine the move of a selected particle, and establish an algorithm for the so called *MFP-kMC*. This is illustrated by three examples using argon as a model fluid: (1) bulk fluid behaviour, (2) vapour-liquid equilibrium and (3) adsorption on a flat graphite surface.

2. Theory

The kinetic Monte Carlo method is described in [1], and it has been shown to be very successful in the description of a number of systems: including gaseous and liquid bulk phases, vapour-liquid equilibria, vapour-solid equilibria, adsorption of argon, nitrogen and carbon dioxide on a graphite surface and in nanopores. With the exception of bulk fluids of infinite extent, the distribution of fluid density is generally non-uniform, making the application of conventional *MC* less efficient because of (1) the small maximum displacement length (which is governed by the dense regions of the system) leading to poor sampling of the rarefied regions and (2) high rejection of attempted moves or insertion in the dense regions. The *kMC* method does not suffer from these disadvantages.

2.1 Potential energies:

Adsorbate-Adsorbate and Adsorbate-Solid potential energies

We use the 12-6 *LJ* equation to describe the pairwise interaction energy between two molecules *i* and *j*:

$$\varphi_{i,j} = 4\varepsilon\left[\left(\frac{\sigma}{r_{i,j}}\right)^{12} - \left(\frac{\sigma}{r_{i,j}}\right)^{6}\right] \tag{1}$$

The solid-fluid potential energy is calculated from Steele 10-4-3 potential energy equation [11, 12]:

$$\phi_{SF} = 2\pi\rho_s\left(\sigma_{SF}\right)^2\varepsilon_{SF}\left[\frac{2}{5}\left(\frac{\sigma_{SF}}{z_i}\right)^{10} - \left(\frac{\sigma_{SF}}{z_i}\right)^{4} - \frac{\left(\sigma_{SF}\right)^4}{3\Delta\left(z_i + 0.61\Delta\right)^3}\right] \tag{2}$$

where Δ is the spacing between two adjacent graphene layers (0.335nm), and ρ_s is the carbon surface density of the graphene layer (38.2nm^{-2}). These potential energy equations are used to illustrate the method that we would like to present in this paper. Any other forms of interaction energy equations could also be used.

Particle energies:

The interaction energy of each molecule *i* with surrounding molecules and the solid surfaces is:

$$u_i = \sum_{\substack{j=1 \\ j\neq i}}^{N}\varphi_{i,j} + \varphi_{i,S} \tag{3}$$

where $\varphi_{i,j}$ is the pairwise interaction energy between molecules *i* and *j*, and $\varphi_{i,S}$ is the interaction energy of molecule *i* and the solid surfaces.

2.2 Models:

2.2.1. Bulk Fluids

The simulation box is a cubic box with periodic boundary conditions imposed on boundaries in all directions.

2.2.2. Vapour-Liquid Equilibrium

The simulation box is a rectangular box containing N particles; the dense phase is placed in the middle of the box and the bulk gaseous phase at the two ends, so that there are two interfaces in the system. Periodic boundary conditions are applied in all directions.

2.2.3. Graphite surface:

The simulation box has linear dimensions of L_x, L_y and L_z, where z is the direction normal to the graphite surface. Periodic boundary conditions are applied in the x and y-directions. The top and bottom of the simulation box are simulated as graphite surfaces.

2.3 Particle mobilities and chemical potential energy

The total mobility of all molecules in the system is expressed by:

$$R = \sum_{i=1}^{N} \nu_i \; ; \qquad \nu_i = \exp\left(\frac{u_i}{kT}\right) \tag{4}$$

where ν_i is the mobility of molecule i. This is a measure of how fast the system evolves, and is inversely proportional to the time that the system spends in a given configuration. The duration Δt of a configuration is independent of any succeeding event, and is given by

$$\Delta t = \frac{1}{R}\ln\left(\frac{1}{p}\right) \tag{5}$$

where p is the random number ($0 < p < 1$).

The chemical potential of the system is calculated from:

$$\mu = kT \ln\left(\Lambda^3 \frac{\overline{R}}{V}\right) \tag{6}$$

where Λ is the thermal de Broglie wavelength and $\overline{R}$ is a time average, calculated from:

$$\overline{R} = \frac{\sum_{j=1}^{M} R_j \left(\Delta t\right)_j}{\sum_{j=1}^{M} \left(\Delta t\right)_j} \tag{7}$$

where M is the number of *kMC* steps. We can also calculate the chemical potential of a particular region by replacing the variables in eq. (6) by those corresponding to that region.

2.4 The Mean Free Path Concept in kMC

The mean speed of a molecule of mass *m* at temperature *T* is given by

$$\overline{v} = \sqrt{\frac{8kT}{\pi m}} \qquad (8)$$

The mean distance between collisions is given by

$$\lambda = \frac{1}{\sqrt{2}\pi\sigma^2\rho} \qquad (9)$$

A particle is chosen according to the Rosenbluth scheme based on the mobility R [1] and given a random direction, which is obtained by the quarternion method [2]. The new position of the particle is selected in a random direction and the distance that it is allowed to travel is:

$$d = \lambda \ln\left(\frac{1}{p}\right) \qquad (10)$$

where *p* is a random number. Eq. (10) is derived from the Beer-Lambert law which gives the probability that a particle will travel a distance *d* as $\exp(-d/\lambda)$. The mean distance travelled after many collisions is:

$$\int_0^\infty x \exp\left(-\frac{x}{\lambda}\right) dx = \lambda \qquad (11)$$

3. Results and Discussion

3.1. Homogeneous Bulk Phase

To study the behaviour of a homogeneous bulk phase using the mean free path (*MFP*) concept in the kinetic Monte Carlo (*kMC*) simulation method, we have chosen argon at 87.3K as an illustrative example. The dimensions of the simulation box are 10 times the collision diameter of argon for all directions, and 2×10^6 and 5×10^6 *kMC* steps are applied for the equilibration and sampling stages, respectively. The results obtained by using conventional *kMC* and the new *MFP-kMC* method are shown in Figure 1 together with the results from the Equation of State (EOS) of Johnson *et al*. [13] which was derived from molecular simulation of LJ molecules. The simulation results from these two schemes agree well with the EOS along the stable vapour and liquid branches. However, in the unstable region there is substantial fluctuation in the *MFP-kMC* results and there is a significant difference between these and the results from the conventional *kMC*. It should be noted that we have used the

same number of *kMC* steps in these two schemes. We attribute these discrepancies to an insufficient number of *kMC* steps in the *MFP* scheme. To test this we increased the number of *kMC* steps to 1×10^7 for both the equilibration and sampling stages. The new simulation results are shown in Figure 2 by the points marked with the symbol ×, where it is clear that the agreement between *MFP-kMC*, conventional *kMC* and the EOS of Johnson *et al*. is much improved, even though there are some modest fluctuations in the unstable region. Simulations with a further increase in the number of *kMC* steps to 2×10^7 and 5×10^7 for equilibration and sampling stages, are shown as the square symbols in Figure 2, and show that the fluctuations in the unstable region are substantially reduced. This example confirms that the *MFP* concept is valid and serves to show that the microscopic origin of the *kMC* method has a basis in the movement of molecules within the framework of the kinetic theory of gases. The key parameter, the mean free path, is calculated from eq. (9) and is inversely proportional to the density of the system.

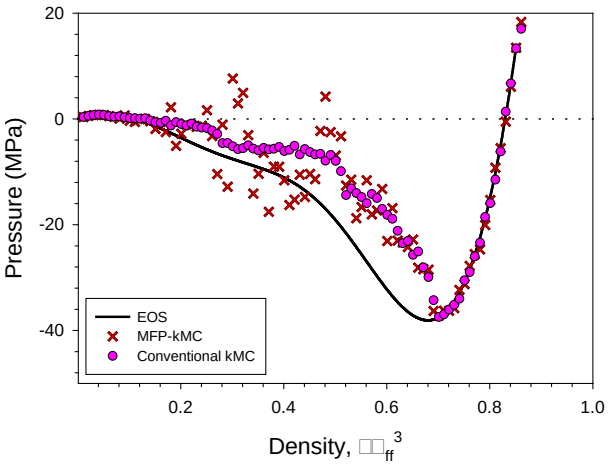

(a)

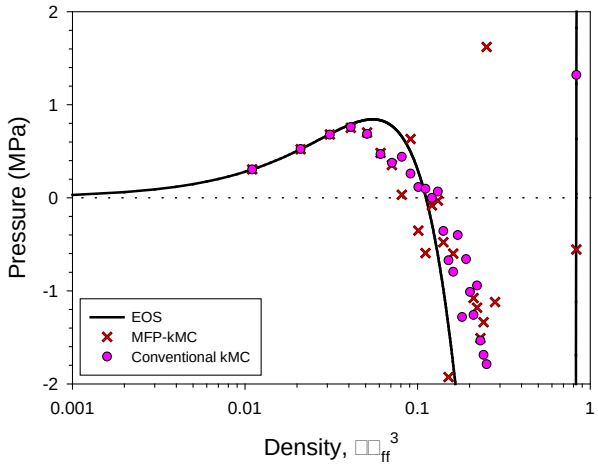

(b)

Figure 1: Argon pressure versus density at 87.3K over the whole pressure/density range: (a) linear scale and (b) semi-logarithmic scale.

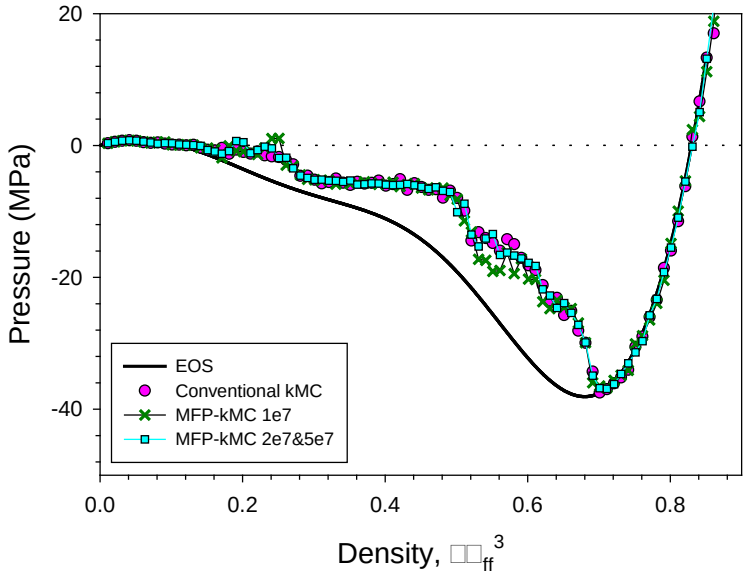

Figure 2: Comparison of Argon pressure versus density at 87.3K obtained with conventional *kMC* and with *MFP-kMC* with longer cycles.

For homogeneous fluids, the density used is the average density in the simulation box. However, for inhomogeneous systems, where density varies from one region to another, it is no longer obvious which density should be used in the calculation of the mean free path. To examine this question we have chosen two examples of inhomogeneous systems; one is the two-phase system of vapour and liquid separated by a flat interface, and the other is adsorption on a graphite surface. Once again, we have used the LJ argon model for these two examples.

3.2. Vapour-Liquid Equilibria

3.2.1 The effects of temperature

The dimensions of the simulation box are $10\sigma \times 40\sigma \times 10\sigma$ (the longest dimension being in the *y*-direction perpendicular to the two interfaces separating a liquid region in the middle from the two gaseous regions). The *kMC* simulation was started with 997 particles arranged at lattice points in the middle of the box such that the initial density equals to the liquid density of argon. For both conventional *kMC* and the *MFP-kMC*, 1×10^7 *kMC* steps were used for both the equilibration and sampling stages. The density distributions in the *y*-direction, in Figure 3, show that these simulation results agree fairly well with each other. The thermodynamic properties derived from these simulations are given in Table 1, together with the experimental data. Both *MFP-kMC* and conventional *kMC* reproduce the experimental data very well, with the exception of the surface tension, which is due to an insufficient number of *kMC* steps for good sampling. The number of *kMC* steps was increased by a

factor of ten to 1×10^8 *kMC*, which leads to excellent agreement with the experimental surface tension as shown in Table 1. It should be noted that in the *MFP-kMC* method, the mean free path calculation was made using the average density of the whole simulation box, irrespective of the volume fraction occupied by the liquid phase in the simulation box.

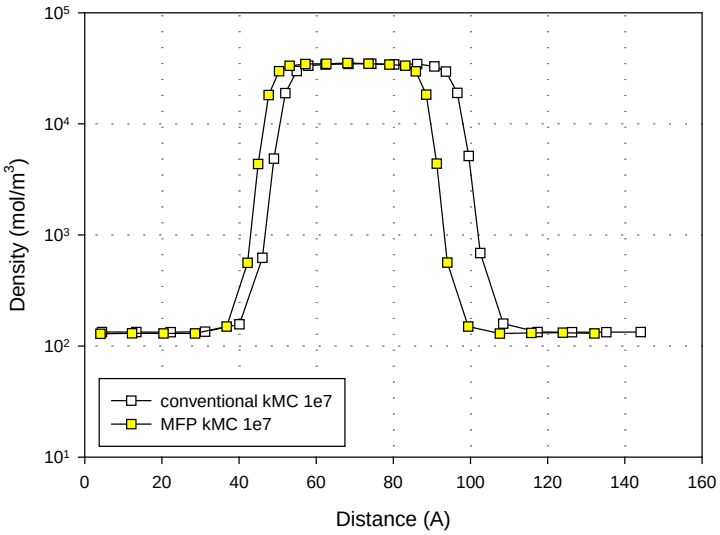

Figure 3: The density profiles of Ar at 87.3K obtained with the *MFP-kMC* and with conventional *kMC*.

Table 1: Thermal properties of argon at 87.3K from *MFP-kMC*, from conventional *kMC* and experimentally. .

	Gas density (mol/m^3)	Liquid density (mol/m^3)	Pressure (Pa)	Phase change heat (kJ/mol)	Surface tension (mJ/m^2)
MFP-kMC (1×10^7)	129	3.50×10^4	9.13×10^4	6.57	6.8
MFP-kMC (1×10^8)	129	3.47×10^4	9.09×10^4	6.53	12.6
kMC (1×10^7)	134	3.47×10^4	9.41×10^4	6.50	9.6
kMC (1×10^8)	132	3.45×10^4	9.28×10^4	6.48	14.2
Experiment	*146	*3.49×10^4	*1.01×10^5	*6.42	12.52 [14]

* data from Perry et al. [15]

Additional *MFP-kMC* simulations were made for Ar at 77K and 100K to further test the capability of the technique in describing the co-existence of bulk fluid argon at different temperatures. The density distributions at 77K are shown in Figure 4 together with the results obtained with *Bin-CMC* developed in our earlier work [16], the two sets of results agree well with each other, except that the gas phase density obtained with *MFP-kMC* is slightly higher than that from *Bin-CMC* method. The bin-CMC were previously shown to be in excellent agreement with Gibbs ensemble MC over the whole coexistence range, including the critical point. Conventional *kMC* simulations were also carried out with the same number

of *kMC* steps for equilibration and sampling as *MFP-kMC*, and the resulting density profile is identical to that obtained with *MFP-kMC*. The thermodynamic properties calculated by *MFP-kMC* are given in Table 2 and compared with the simulated data from conventional *kMC* and *Bin-CMC*.

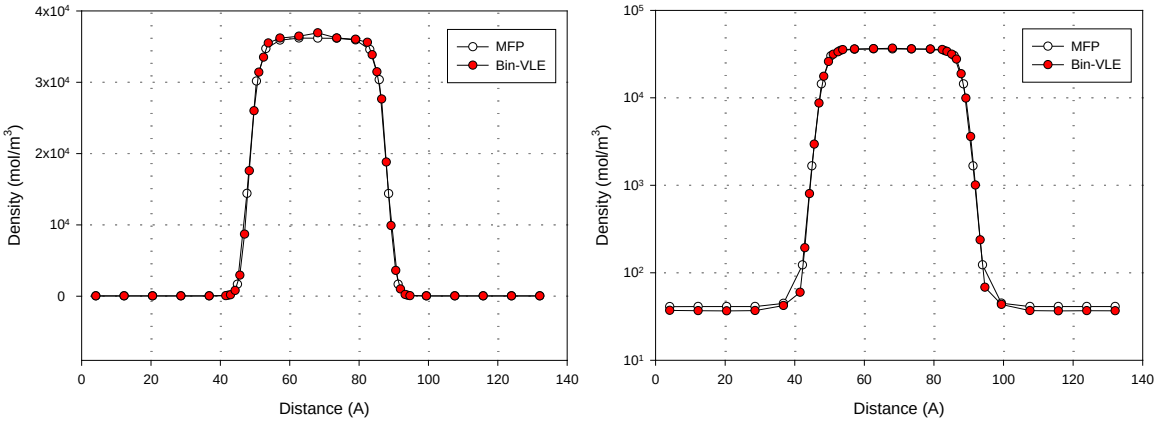

Figure 4: The density profiles of Ar at 77K obtained with the *MFP-kMC* and comparison with that obtained with the *Bin-CMC*.

Table 2: Thermodynamics properties of argon at 77K from *MFP-kMC* and comparison with conventional *kMC* and *Bin-CMC* data.

	Gas density (mol/m^3)	Liquid density (mol/m^3)	Pressure (Pa)	Phase change heat (kJ/mol)	Surface tension (mJ/m^2)
MFP-kMC	41	3.62×10^4	2.60×10^4	6.80	14.8
Conventional kMC	42	3.59×10^4	2.65×10^4	6.76	11.9
Bin-CMC	37	3.65×10^4	2.35×10^4	6.87	15.3

The results obtained at 100K show similar trends to those already discussed for lower temperatures. They are plotted in Figure 5 and tabulated in Table 3, together with the experimental data.

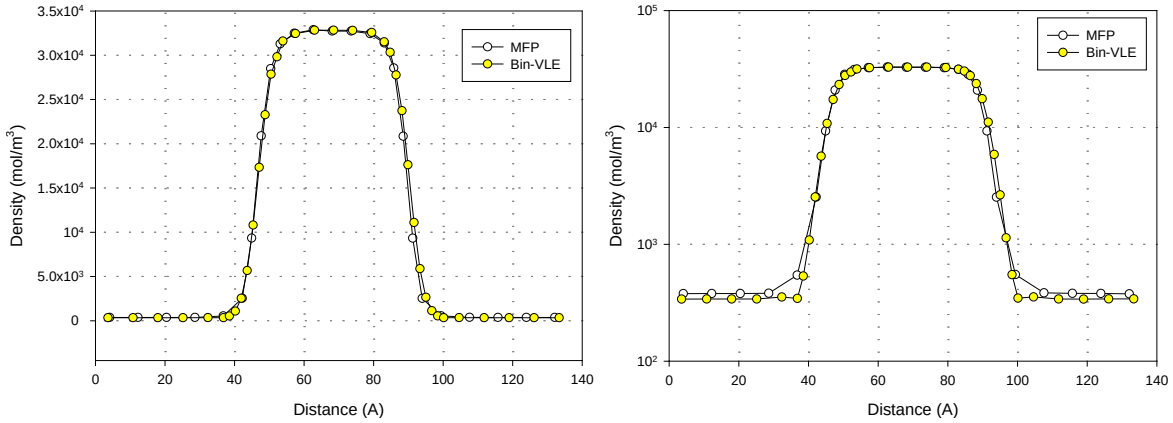

Figure 5: The density profiles of Ar at 100K obtained with the *MFP-kMC* and comparison with that obtained with the *Bin-CMC*.

Table 3: Thermal properties of argon at 100K from *MFP-kMC* and comparison with the conventional *kMC*, *Bin-CMC* and experimental data.

	Gas density (mol/m^3)	Liquid density (mol/m^3)	Pressure (Pa)	Phase change heat (kJ/mol)	Surface tension (mJ/m^2)
MFP-kMC	378	3.27×10^4	2.94×10^5	6.14	10.5
Conventional kMC	379	3.27×10^4	2.95×10^5	6.14	10.4
Bin-CMC	340	3.29×10^4	2.68×10^5	6.18	10.3
Experiment	*426	*3.28×10^4	*3.25×10^5	*6.00	9.4 [14]

* data from Perry et al. [15]

3.2.2 The effects of box size

To test the effects of box size we extended the simulation box of Section 3.2.1 by adding 3nm to both gaseous regions in the *y* direction; keeping the same number of particles. The density profiles in this new box are shown as green circles in Figure 6, and it can be seen that the gas phase and liquid phase densities are not affected by the box size. The density profiles obtained when a further 3nm was added to both sides of the box along the *y* direction is shown as red circles in Figure 6 and confirms that both densities are unaffected. The density profiles obtained with the largest simulation box for 77 and 100K are shown in Figures 7 and 8, respectively; and once again confirm that the box size does not affect the results or the derived thermodynamic properties.

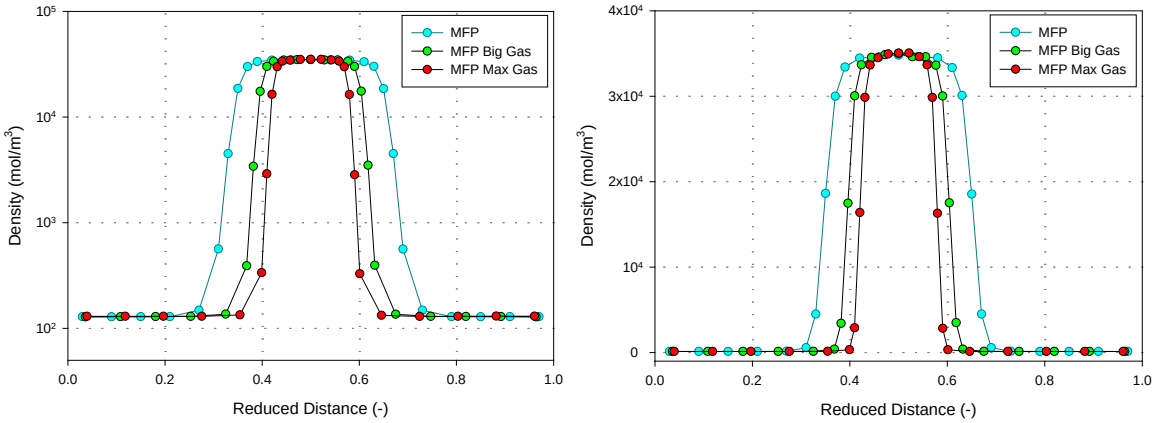

Figure 6: The density profiles of Ar at 87.3K obtained with different sizes of the gas phase zone keeping the total number of particles in the box constant.

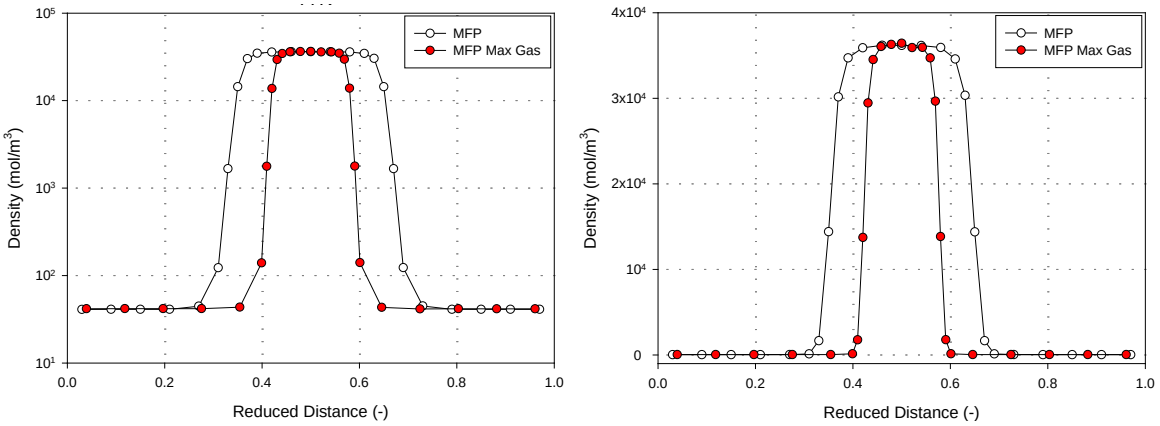

Figure 7: The density profiles of Ar at 77K obtained with different sizes of the gas phase zone, keeping the total number of particles in the box constant.

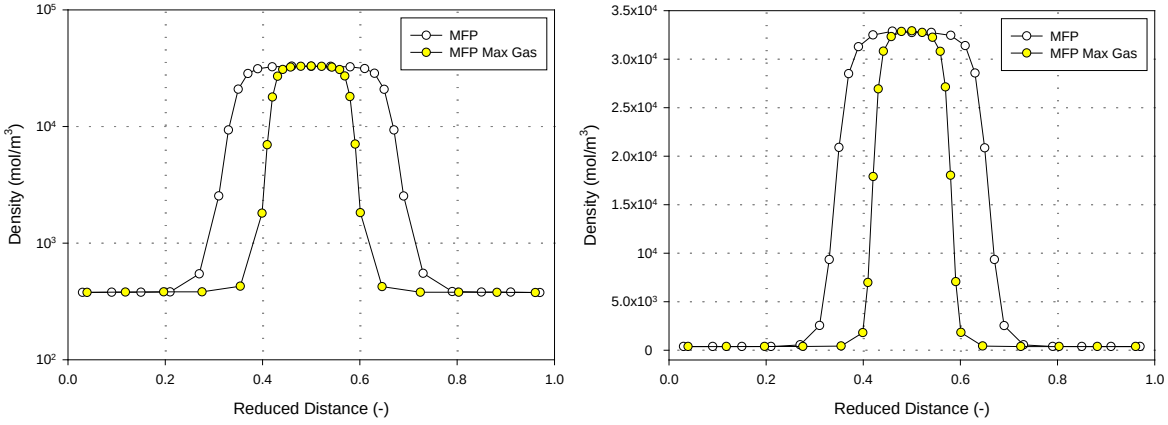

Figure 8: The density profiles of Ar at 100K obtained with different sizes of the gas phase zone keeping the total number of particles in the box constant.

3.3. Single Particle on Graphite Surface

The box dimensions are 10nm×10nm×10nm for L_x, L_y and L_z, respectively. The bottom and top surfaces, normal to the *z*-axis, are bound by graphite walls and periodic boundary

conditions are applied in the *x* and *y* directions. If the molecule moves out of the simulation box via the top or bottom graphite surface, that move is rejected and the old configuration is recounted for the time averaging in the sampling stage; this is then followed by giving the molecule a new random direction and a new distance to travel (according to eq. 10) until a new position in the box can be found. The density profile collected in the sampling stage is shown in Figure 9. The Boltzmann distribution calculated as $\rho = \rho_\infty e^{(-\varphi_{SF}/kT)}$ (symbols ×) is also plotted on the same graph, where ρ_∞ is the density far away from the surface and φ_{SF} is the potential energy between the molecule and the graphite surface. Figure 9 shows that the *MFP-kMC* density distribution profile exactly matches the Boltzmann distribution, and therefore the *MFP-kMC* procedure produces the correct distribution of particles at zero loading.

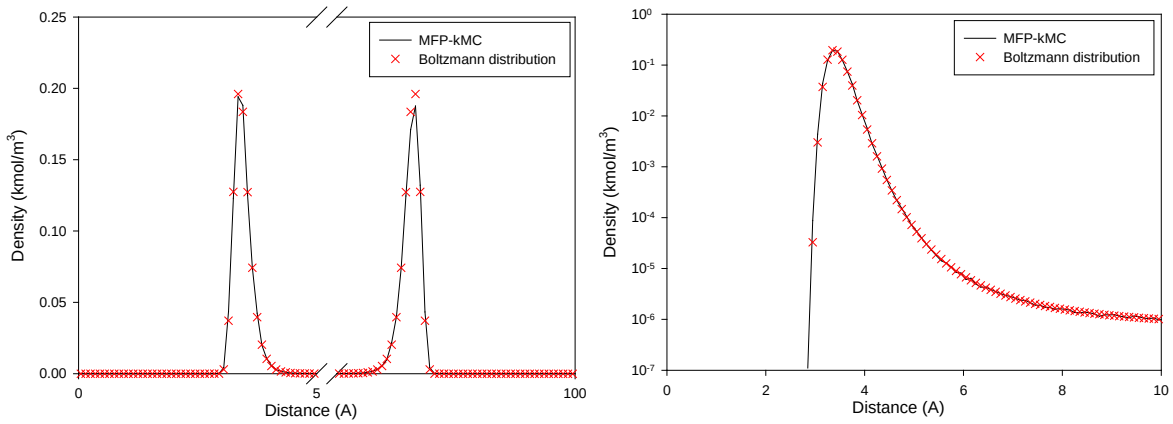

Figure 9: The density distribution profile for one argon particle on two graphite surfaces in a 10nm cubic box at 87.3K.

3.4. Adsorption on Graphite Surface

The *MFP-kMC* was next applied to adsorption of Ar on a graphite surface at 87.3K. The simulation box was set up with two graphite surfaces represented by the Steele potential (eq. (2)) at each boundary in the *z*- direction and the box height was chosen large enough that this system is equivalent to one with two independent surfaces. The use of a graphite surface at both boundaries avoids the sharp drop in the density profile that occurs at a hard wall at high mean densities, due to the absence of molecules at the boundary and beyond. The dimensions of the simulation box are set as 34.05×34.05×10nm, the section, parallel to the *xy*-plane, of 2nm thickness in the middle of the box is treated as the bulk gas phase, and used to evaluate the relevant properties of the gas phase.

When a selected molecule crosses the boundary in the *z*-direction, the move is rejected and the old configuration is recounted in the time averaging; the molecule is then given a new random direction and a new distance to travel until its path remains within the box. We used 2×10^6 and 5×10^6 *kMC* steps for the equilibration and sampling stages, respectively. The isotherms obtained with *MFP-kMC* and conventional *kMC* (using the same number of steps as *MFP-kMC*) are plotted in Figure 10; the experimental data are also shown in the same figure for comparison with the simulation results. On the logarithmic scale of Figure 10a, it can be seen that the *MFP-kMC* simulation agrees well with conventional *kMC* in the monolayer region. To show the results at higher coverage more clearly the data are plotted on a linear scale in Figure 10b, and it can be seen that the results from the *MFP-kMC* are in excellent agreement with conventional *kMC* in this coverage region.

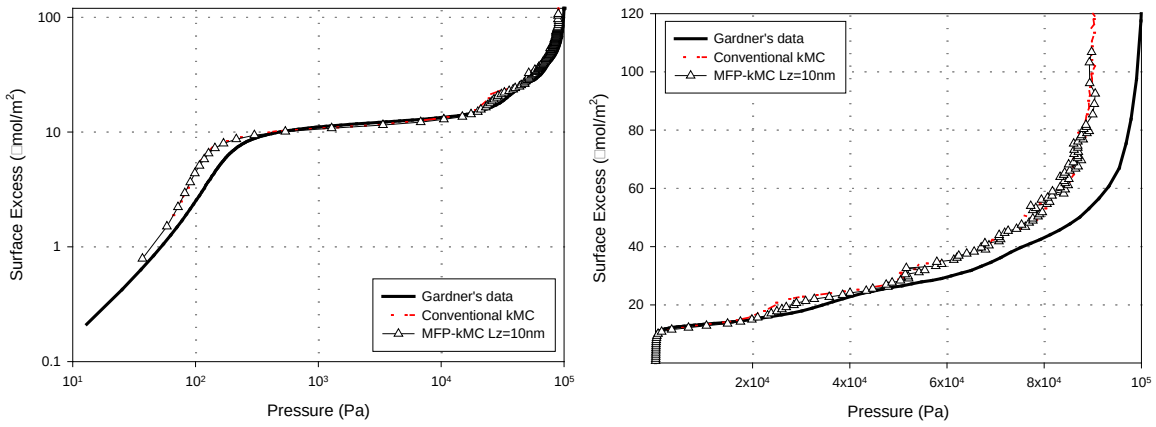

Figure 10: The adsorption isotherms for argon on a graphite surface at 87.3K obtained with *MFP-kMC* and conventional kMC, and the experimental data of Gardner et al. (a) logarithm scale, (b) linear scale.

To investigate the effects of the box size, we doubled the box height to 20nm, and increased the number of *kMC* steps by a factor of ten (i.e. 2×10^7 for equilibration and 5×10^7 for sampling). The results obtained with *MFP-kMC* using the larger box are shown in Figure 11. The isotherm agrees well with the conventional *kMC* results in the monolayer region, but it slightly shifts to higher pressures in the multilayer regions. A further increase (by an order of magnitude) in number of *kMC* steps gave identical results

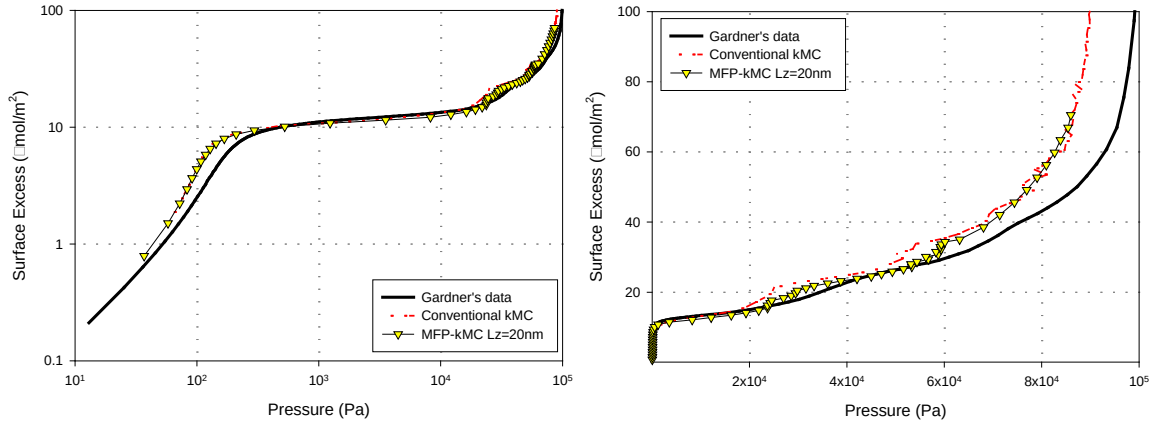

(a) (b)

Figure 11: The adsorption isotherms for argon on graphite at 87.3K obtained using *MFP-kMC* in a simulation box with size of 34.05×34.05×20nm. The experimental data of Gardner et al are shown for comparison, (a) logarithm scale, (b) linear scale.

4. Conclusions

In this work, we have investigated the mechanics of the displacement of particle in the *kMC* method by introducing in the concept of mean free path (*MFP*), and sampled the travel distance of a particle calculated from the Beer-Lambert law. The *MFP-kMC* scheme was tested with various systems, including the homogeneous bulk phase, vapour-liquid equilibrium and adsorption on graphite surfaces. For all these systems, good agreement is achieved between the new scheme and conventional *kMC*, confirming that the particle displacement can be calculated as the distance travelled between two successive collisions, in accordance with the kinetic theory.

Acknowledgement: This work is supported by the Australian Research Council

References

1. Ustinov, E. A. and Do, D. D., *Application of kinetic Monte Carlo method to equilibrium systems: Vapour–liquid equilibria.* Journal of Colloid and Interface Science, 2012. 366(1): p. 216-223.
2. Allen, M. P. and Tildesley , D. J., *Computer Simulation of Liquids*. 1989, Oxford: Oxford University Press. xiii, 385.
3. Frenkel, D. and Smit, B., *Understanding Molecular Simulation : From Algorithms to Applications.* 1996, San Diego: Academic Press. xviii, 443.
4. Bortz, A. B., Kalos, M. H. and Lebowitz, J. L., *A new algorithm for Monte Carlo simulation of Ising spin systems.* Journal of Computational Physics, 1975. 17(1): p. 10-18.
5. Gillespie, D. T., *Exact stochastic simulation of coupled chemical reactions.* The Journal of Physical Chemistry, 1977. 81(25): p. 2340-2361.
6. Voter, A. F., *Classically exact overlayer dynamics: Diffusion of rhodium clusters on Rh(100).* Physical Review B, 1986. 34(10): p. 6819-6829.
7. Fichthorn, K. A. and Weinberg, W. H., *Theorecical Foundations of Dynamic Monte-Carlo Simulations.* Journal of Chemical Physics, 1991. 95(2): p. 1090-1096.
8. Battaile, C., *The Kinetic Monte Carlo method: Foundation, implementation, and application.* Computer Methods in Applied Mechanics and Engineering, 2008. 197(41-42): p. 3386-3398.
9. Rowlinson, J. S. and Widom, B., *Molecular theory of capillarity*. 1982, Oxford, Oxfordshire :: Clarendon Press. xi, 327 p :.
10. Bennett, C. H., *Efficient estimation of free energy differences from Monte Carlo data.* Journal of Computational Physics, 1976. 22(2): p. 245-268.
11. Steele, W. A., *The physical interaction of gases with crystalline solids: I. Gas-solid energies and properties of isolated adsorbed atoms.* Surface Science, 1973. 36(1): p. 317-352.
12. Steele, W. A., *International Encyclopedia of Physical Chemistry and Chemical Physics, Topic 14, Vol. 3: The Interaction of Gases with Solid Surfaces.* 1974: Pergamon. 356 pp.
13. Johnson, J. K., Zollweg, J. A. and Gubbins, K. E., *The Lennard-Jones equation of state revisited.* Molecular Physics: An International Journal at the Interface Between Chemistry and Physics, 1993. 78(3): p. 591 - 618.
14. Wohlfarth, C. and Wohlfarth, B., *Pure Liquids: Data. SpringerMaterials - The Landolt-Börnstein Database (http://www.springermaterials.com)*, ed. M.D. Lechner. Vol. 16: Surface Tension of Pure Liquids and Binary Liquid Mixtures
15. Perry, D. W. and Robert H.; Green, *Perry's Chemical Engineers' Handbook.* Seventh Edition ed. 1997: McGraw-Hill.
16. Fan, C., Do, D. D. and Nicholson, D., *New Monte Carlo Simulation of Adsorption of Gases on Surfaces and in Pores: A Concept of Multibins.* The Journal of Physical Chemistry B, 2011. 115(35): p. 10509-10517.